
**STRENGTH
AND PLASTICITY**

Effect of the Strain and Strain Rate on Microstructure Evolution and Superplastic Deformation Mechanisms

O. A. Yakovtseva^a*, A. V. Mikhaylovskaya^a, A. D. Kotov^a, O. I. Mamzurina^a, and V. K. Portnoy^a

^a*Department of the Metallurgical Science of Nonferrous Metals, National University of Science and Technology MISiS, Moscow, 119049 Russia*

**e-mail: yakovtseva.o@mail.ru*

Received March 21, 2018; revised May 23, 2018

Abstract—Parameters of superplasticity of the Al–7.6% Mg–0.6% Mn–0.25% Cr alloy have been studied in the range of 490–520°C, and the optimum temperature of deformation has been determined. The evolution of the grain structure in the bulk and on the surface of samples during the superplastic deformation at a temperature of 510°C has been analyzed. The contribution of grain-boundary sliding has been estimated in the strain-rate regime of superplastic deformation according to the results of the analysis of changes in the structure of the surface with preliminarily applied marker scratches. The contribution of grain-boundary sliding to the total deformation is 20–30%; the contribution of diffusion creep decreases from 40 to 20% with an increase in the deformation rate by an order of magnitude, from 1×10^{-3} to $1 \times 10^{-2} \text{ s}^{-1}$. The intragranular deformation is localized in the peripheral regions of grains and in the region of striated zones.

Keywords: superplasticity, aluminum alloys, grain-boundary sliding, diffusion creep, dislocation structure

DOI: 10.1134/S0031918X18110224

INTRODUCTION

Superplasticity is the ability to undergo a significant quasi-uniform deformation in a specific temperature–strain-rate range due to a high sensitivity of the flow stress to the deformation rate. The state of superplasticity is inherent in alloys with an average grain size less than $10 \mu\text{m}$ [1, 2]. The relative elongation of samples upon superplastic deformation under optimum conditions can reach hundreds and even thousands of percent [3, 4]. This effect is used in the fabrication of articles of complex shapes by the method of superplastic forming. The significant gain in strain makes it possible to produce details of a complex shape with a fine relief. To guarantee the efficiency of the superplastic forming of aluminum alloys, it is necessary to ensure high elongations at the maximum possible deformation rate. For aluminum alloys utilized in industry, strain rates in the interval of 10^{-4} – 10^{-3} s^{-1} are typically used. Optimum conditions for forming alloy AA5083, which contains about 5.0 wt % Mg, and is the most widely used in industry, are as follows: a temperature of 520–550°C; and a rate of deformation near $(1–2) \times 10^{-3} \text{ s}^{-1}$; in this case, the relative elongation reaches 300–350% [5–9]. An increase in the strain-rate range of the superplasticity by an order of magnitude will ensure a rise in the productivity of the method and, therefore, the expansion of the fields of its application. As has been shown in a number of works [10–13], an increase in the magnesium content to a certain limit

leads to an improvement in the indices of superplasticity, including an increase in the strain-rate range of the appearance of the effect. Thus, the alloy with 6.8 wt % Mg [14] with a small contribution of grain boundary sliding shows up elongations close to 350–400% at a deformation temperature of 520°C and at a considerably higher optimum rate of deformation of $5 \times 10^{-3} \text{ s}^{-1}$. In this case, the superplasticity in the alloys that contain up to 7 wt % magnesium has been investigated in detail; the alloys with greater contents of Mg have been studied in less detail.

Note that for forming materials under superplasticity conditions we must know not only about optimum regime of deformation, i.e., the temperature, strain rate, and the value of the flow stress, but also about the structural changes—evolution of the grain structure and porosity upon the deformation. These parameters are responsible for a change in the stress value upon the forming, and, also affect the final properties of the details. The structural changes upon the superplastic flow are determined by the chemical and phase composition of the alloys and partly depend on the acting mechanisms of deformation. Despite the large number of experimental and theoretical studies [3, 4, 15–17], there is no consensus about the main and accommodation mechanisms that ensure the high strain-rate sensitivity of the flow stress and the superplastic state. The grain-boundary sliding (GBS) is usually considered to be the dominant mechanism [2, 4].

A large contribution of GBS (to 50–80%) has been confirmed for some aluminum alloys, for example, AA7075 and its analog AA7475 [18–20], alloys of eutectic type [21, 22], and other two-phase alloys [16, 23, 24]. Note that the alloys with a developed GBS show significant residual porosity after deformation [25, 26]. On the contrary, some aluminum alloys demonstrate a small contribution of grain-boundary sliding (10–20%) [3, 27] and a low residual porosity [28, 29], for example, Al–Mg alloys. As has been shown in a number of works [3, 16], the basic mechanism of the superplastic deformation of the AA5083 type alloys is diffusion creep. Estimations based on the width of zones free of precipitates formed upon deformation, which are considered the structural sign of diffusion creep [30], allow the authors to assume that the contribution of diffusion creep to the total elongation can reach 50%. The acting mechanisms of deformation in the alloys with high contents of magnesium have been investigated in little detail.

This work is aimed at a study of the deformation behavior in the superplastic state, the evolution of the structure, and the contributions of the acting mechanisms of deformation in the alloy with an enhanced content of magnesium, 7.6% Mg–0.6% Mn–0.25% Cr, at different rates of superplastic deformation.

EXPERIMENTAL

The alloy under investigation has the following composition: Al–7.6% Mg–0.6% Mn–0.25% Cr. Sheets of the alloy were manufactured under laboratory conditions. To obtain ingots, we used the following materials: aluminum of grade A99; magnesium of grade Mg95; and master alloys Al–10% Mn, and Al–10% Cr. The melts were poured into a copper water-cooled mold with dimensions of $100 \times 40 \times 20$ mm. The homogenization annealing was carried out in a Nabertherm N 30/65 A furnace in two steps, with holding at 430°C for 4 h; and at 460°C for 4 h. Hot rolling with a reduction to 70% was carried out at a temperature of $420 \pm 20^\circ\text{C}$. Then, rolling was performed at room temperature to the final thickness of the sheet equal to 1 mm.

Samples for the analysis of the microstructure were prepared with the aid of mechanical grinding and polishing with a subsequent electropolishing in a chloric acid–alcohol electrolyte at a voltage of 14 V for 5–7 s. To reveal the grain structure, we performed additional oxidizing in a 10% aqueous solution of hydrofluoric acid under a voltage of 25 V for 20–30 s.

The microstructure was investigated with the aid of a Neophot-30 optical microscope. The grain size was characterized with the value of a mean chord along and across the rolling direction, which we measured using the random-intercept method.

The superplasticity indices were determined using a Walter Bay LFM-100 tensile testing machine on

samples with a length of the gage part of 14 mm, a width of 6 mm, and a thickness of 1 mm [31]. The tests were conducted with a stepped increase in the strain rate in the 490–520°C temperature range with a step of 10 K and in the interval of strain rates of 5×10^{-5} to $5 \times 10^{-2} \text{ s}^{-1}$ for the determination of the index of the strain-rate sensitivity m and of the strain-rate range of superplasticity.

The dislocation structure was studied with the aid of a JEOL JEM-2100 transmission electron microscope. The samples for the study were electrolytically thinned using a TenuPol setup and the electrolyte A2 at a voltage of 20 V.

The analysis of structural changes on the surface of the samples was carried out before and after the deformation with the aid of a TESCAN Vega 3 LMH scanning electron microscope. To determine the contribution of the GBS, we applied marker scratches on the preliminarily polished sample of the alloy perpendicular to the tensile axis using a three-micron diamond paste. The displacements of the scratches were analyzed after sequential deformation to 13, 35, and 70% [32]. The deformation of samples with marker scratches was carried out in an argon atmosphere to decrease the oxidation of the surface.

RESULTS AND DISCUSSION

In the heating process and 20-min holding in the 490–520°C temperature range, a recrystallized grain structure is formed in the sheets (Fig. 1). The size of the recrystallized grain does not change within the limits of a measurement error in the investigated temperature range of annealing and is 6.7 to 7.3 μm , i.e., on average, is $7.0 \pm 0.3 \mu\text{m}$; thus, before the beginning of deformation, a rather uniform grain structure is formed.

To determine the superplasticity indices of the alloy from the test results with a stepped increase in the strain rate, we constructed graphs of the dependence of the flow stress and strain-rate sensitivity m on the strain rate (Figs. 2a, 2b). The dependence of the stress on the deformation rate has a sigmoid shape typical of the superplastic alloys. The value of stress decreases regularly as the temperature of tests increases from 490 to 520°C (Fig. 2a). The deformation rate, which corresponds to the maximum values of m , is $2 \times 10^{-3} \text{ s}^{-1}$ at temperatures of 490–500° and increases to $5 \times 10^{-3} \text{ s}^{-1}$ at temperatures of 510–520°C (Fig. 2b). At a temperature of 510°C, the alloy demonstrates a higher strain-rate sensitivity, and the index m is ≥ 0.5 in the widest interval of rates, from 8×10^{-4} to $2 \times 10^{-2} \text{ s}^{-1}$.

To study the structural changes and analysis of the contributions of the acting mechanisms of deformation, we selected a temperature of 510°C, which corresponds to $0.97 T_m$ on the homologous scale, and the strain rates 1×10^{-3} , 5×10^{-3} , and $1 \times 10^{-2} \text{ s}^{-1}$ within the limits of the linear segment of the σ – $\dot{\epsilon}$ depen-

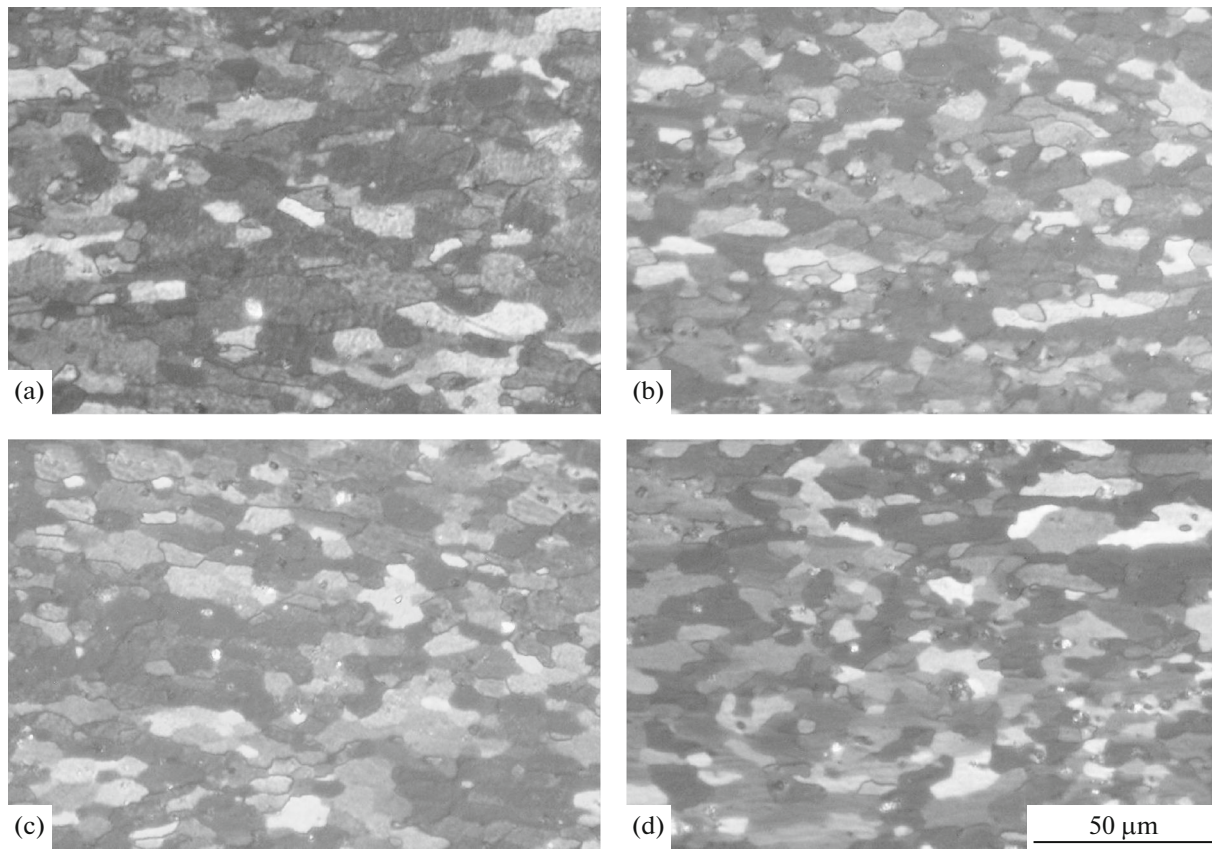


Fig. 1. Grain structure after 20-min annealing at temperatures of (a) 490, (b) 500, (c) 510, and (d) 520°C.

dence. The relative elongations were $600 \pm 10\%$, $450 \pm 10\%$, and $290 \pm 10\%$ at the temperature of 510°C and the strain rates of 1×10^{-3} , 5×10^{-3} , and $1 \times 10^{-2} \text{ s}^{-1}$, respectively (Fig. 2c). The dependence of the stress on the deformation at the investigated rates (1×10^{-3} , 5×10^{-3} , and $1 \times 10^{-2} \text{ s}^{-1}$) is shown in Fig. 2c. The maximum values of the stress increase regularly from 8 to 16 MPa with an increase in the strain rate by an order of magnitude.

In the deformation curves at the strain rates of 1×10^{-3} and $5 \times 10^{-3} \text{ s}^{-1}$, we can separate two stages: the stage of strain hardening; and the stage of a steady flow, where the stress weakly depends on deformation. At the rate of deformation equal to $1 \times 10^{-2} \text{ s}^{-1}$, the stage of steady flow is absent; we observed an essential softening and the absence of a pronounced neck in the sample instead. The shape of the deformation curves is determined to a significant extent by structural changes under the deformation, including the evolution of the grain structure and the porosity. The steady flow can be connected with both the stable grain size upon the domination of grain-boundary sliding and with the development of the processes of dynamic recrystallization or with the development of the porosity, which leads to a decrease in the “clear” section of the sample.

The longitudinal average dimension of the grains is increased by a factor of 1.5–1.6, from 6.8 to 10–11 μm , upon the deformation to failure at all investigated strain rates (Fig. 3). The grains are elongated at the initial stage of the deformation; the shape factor (ratio of the transverse to the longitudinal grain size) decreases from 0.64 to 0.54 during the first 100% of deformation and almost does not change further. At the strain rates of 1×10^{-3} and $5 \times 10^{-3} \text{ s}^{-1}$, the grains grow approximately up to the degree of deformation equal to 300%; then, the grain size does not change up to failure at 600 and 450%, respectively (Fig. 3). With an increase in the strain rate to $1 \times 10^{-2} \text{ s}^{-1}$, the dynamic grain growth occurs more intensively and can be observed up to the failure. The rate of the dynamic grain growth is 0.2, 0.7, and 2 $\mu\text{m}/\text{min}$ at the strain rates of 1×10^{-3} , 5×10^{-3} , and $1 \times 10^{-2} \text{ s}^{-1}$, respectively; i.e., with an increase in the strain rate by an order of magnitude, the rate of grain growth also increases by an order of magnitude.

A porosity was seen at a deformation of 100% in the structure of the sample stretched at a rate of $1 \times 10^{-2} \text{ s}^{-1}$, while at the other rates, the deformation to 100% did not lead to the formation of pores. At the strain rates of 1 and $5 \times 10^{-3} \text{ s}^{-1}$, the porosity is developed only after the deformation to 350–400%.

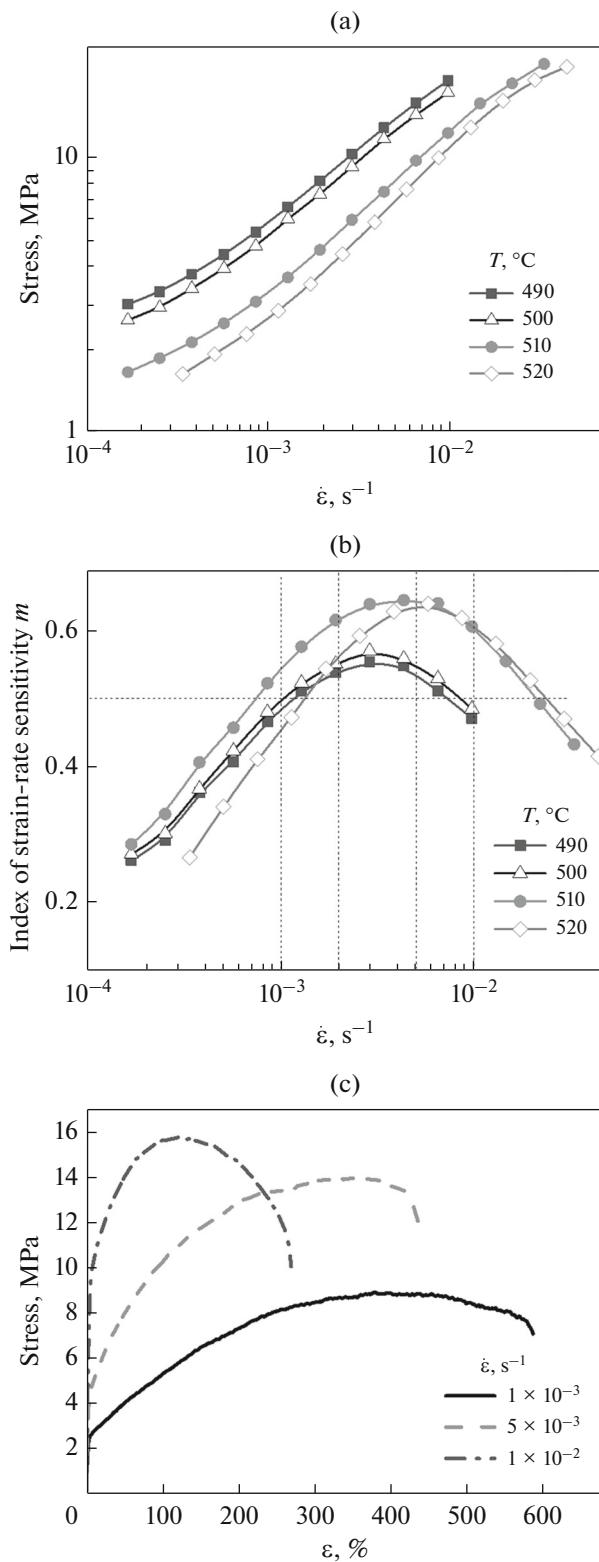


Fig. 2. Dependences of (a) the stress and (b) the strain-rate sensitivity index m on the deformation rate in the range of temperatures of 490–520°C, and (c) the stress–strain curve at the temperature of 510°C and different constant strain rates.

The strain-induced hardening at the initial stage, at the strain rates of 1 and 5×10^{-3} s^{-1} , can be connected with the dynamic grain growth, while at the stage of the steady flow, where the stress is constant, the grain size also does not change. The softening upon the deformation more than 100% at a strain rate of 1×10^{-2} s^{-1} is likely connected with the intensive development of porosity; as a result, the increase in the values of the flow stress, which must occur due to grain growth, is overlaid by the reduction in the flow stress because of the decrease of the “clear” section of the sample due to the pore formation.

Grain growth can have a dislocation or diffusion nature and it can also be caused by the migration of grain boundaries. In the structure of samples deformed at different strain rates, particle-depleted zones (PDZ) are seen, which are formed near the triple joints of grains and at the transverse boundaries (dashed arrows in Fig. 4). Such zones are considered the basic sign of diffusion creep. We carried out the comparative quantitative analysis of the volume fraction of PDZ at different deformation rates, i.e., in essence, the analysis of the contribution of diffusion creep to the total strain, after 100-% deformation. With an increase in the deformation rate, the contribution of the diffusion creep decreases from 40% at the strain rate of 1×10^{-3} s^{-1} to 30% at 5×10^{-3} s^{-1} and to 20% at 1×10^{-2} s^{-1} .

We can assume that an increase in the grain size occurs at the beginning of deformation mainly due to the diffusion mass transfer.

We analyzed the dislocation structure before the beginning of deformation and also after 50- and 100-% deformation at all strain rates. In the samples studied before the beginning of deformation (after 20-min annealing at a temperature of 510°C, Fig. 5a), the dislocations in the bulk of grains were virtually absent.

After the superplastic deformation, we observed signs of dislocation activity; the formation of dislocation walls occurs (Figs. 5b, 5c, 5d), i.e., dynamic polygonization takes place. No substantial differences were seen in the dislocation structure of the alloy depending on the rate of superplastic deformation up to 50% and 100% deformation. The enhanced dislocation activity allows us to assume the action of intragranular dislocation creep as one of the mechanisms of superplastic deformation, may be, of accommodation nature, in the interval of strain rates investigated.

The basic method, which allows us to analyze the acting mechanisms of superplastic deformation, is the analysis of the evolution of the structure of the surface. We studied changes in the surface of samples with marker scratches at a temperature of 510°C and strain rates of 1×10^{-3} , 5×10^{-3} , and 1×10^{-2} s^{-1} . Figure 6 demonstrates the evolution of the structure of the fragments of the surface of samples with marker scratches after sequential deformation to 13, 35, and 70%. Even

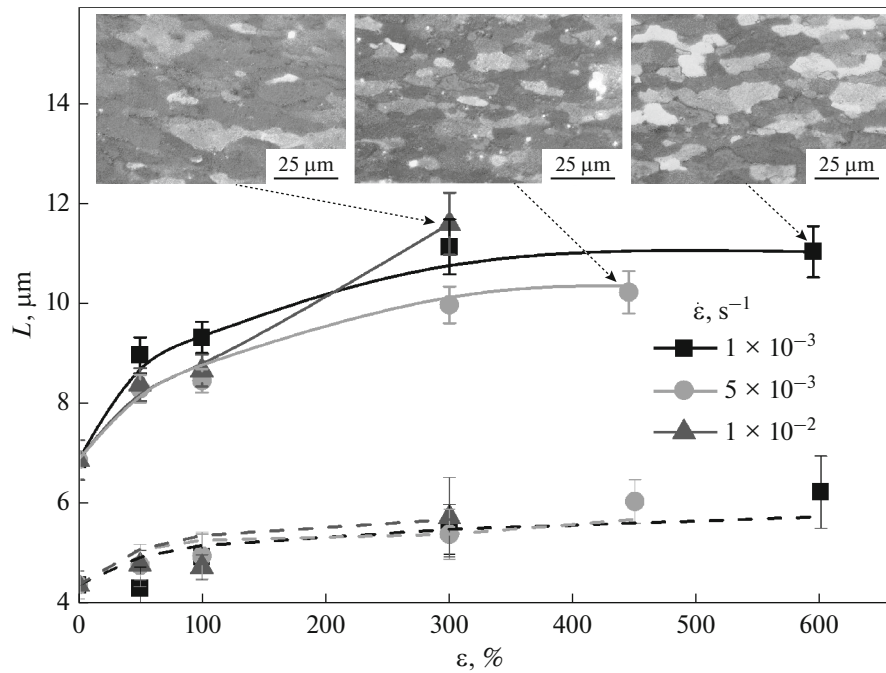


Fig. 3. Dependence of the grain size on the degree of deformation at a temperature of 510°C (solid lines correspond to the longitudinal size of the grains; dashed lines, to the transverse size of grains).

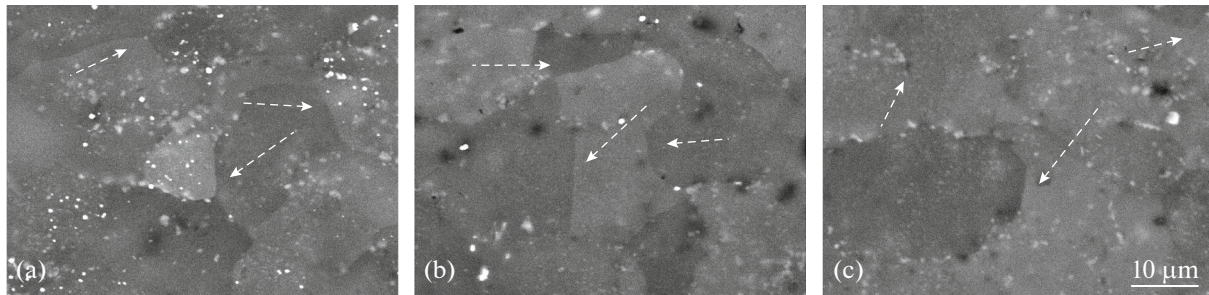


Fig. 4. Microstructure of the sample after 100-% deformation at strain rates of (a) 1×10^{-3} , (b) 5×10^{-3} , and (c) $1 \times 10^{-2} \text{ s}^{-1}$; dashed arrows indicate zones free of precipitates.

after 13-% deformation, at the surface of the samples a relief appears (Figs. 6a, 6d, 6g) and displacements of scratches along the boundaries of the grains occur (shown by dashed lines), i.e., we observed characteristic features of GBS. With an increase in the degree of deformation, the magnitude and the number of displacements of marker scratches grow, a rotation of grains occurs (X), and the displacement of grains into the bulk of the sample (E) is observed.

We calculated the contribution of the GBS to the total deformation based on the displacement of marker scratches for the compared deformation rates. With an increase in the deformation rate by an order of magnitude, the contribution of the GBS decreases from 30 to 20% (Fig. 6) upon the total deformation of 13%. With an increase in the deformation to 70%, the contribution of the GBS is 20% at both investigated rates.

Note that the “neighbor switching” in the alloy investigated even at the low rate of deformation is pronounced considerably weaker than, for example, in the alloy AA7475 [20]. The grains A, B, C, and D in Fig. 6 do not move significantly relative to initial positions in the case of the 70-% total deformation. This refers also to the remaining neighboring grains. The authors of [3] noted that no change in the neighbors of grains was seen in the AA5083 alloy; the authors of [17] believe that the change of neighbors occurs, but is obscured by the deposits of oxides on the surface of the sample. The deformation to 70% may be insufficient for the appearance of this transposition of grains in the alloy investigated.

The intragranular deformation caused by the action of diffusion and dislocation creep can be estimated based on the changes in the geometry of

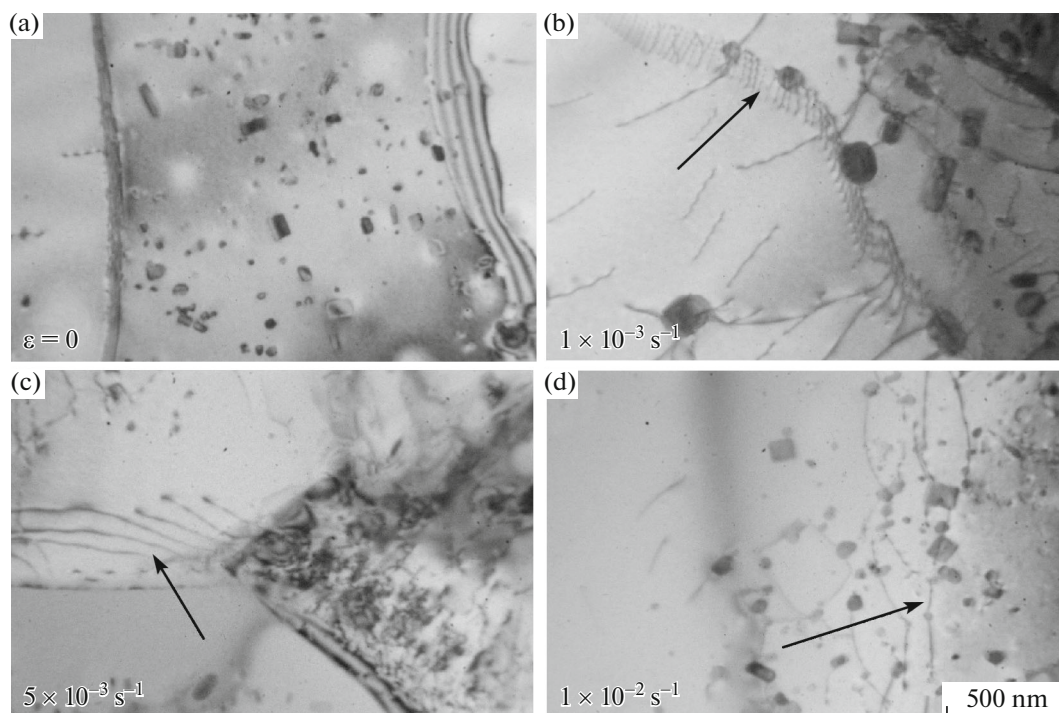


Fig. 5. Dislocation structure (a) after annealing for 20 min at a temperature of 510°C and after deformation to 100% at strain rates of (b) 1×10^{-3} , (c) 5×10^{-3} , and (d) $1 \times 10^{-2} \text{ s}^{-1}$.

scratches within the limits of one grain. As we can see from Fig. 6, we did not observe any smearing of scratches or change in the distance between the scratches in the bulk of grains. The marker scratches are eroded only in the regions of striated (folded) zones (Figs. 6a–6c, arrows), where deformation is localized. These zones are mainly oriented along the tensile axis and are located near the transverse grain boundaries. Such zones appear after the 13-% deformation and become more clearly pronounced and wide with an increase in the deformation to 70%. The reasons for the appearance of striated zones in the alloy of the same system of alloying as in AA5083 is discussed by the authors of [17], who concluded that the striated zones are the consequence of diffusion mass transfer and of the growth of the oxide on the freshly formed surface of the sample. The stepped growth characteristic of the aluminum oxide, according to the data of [17], can create the effect of folding on the surface. The analysis of material under the folded zone reveals the presence of particle-depleted zones, which are considered a sign of diffusion creep. The same conclusions about the nature of the appearance of striated zones upon the superplastic deformation were made earlier based on the results of the analysis of replicas by the authors of [22] for the alloys of other systems.

As no signs of the deformation of the grain bulk were revealed on the surface of the samples, we can assume that the dislocation creep, just as the diffusion

mass transfer, can be localized only in the periphery of grains, in the striated zones, or in the grain “mantle” according to Jifkins.

The intensive grain growth at the initial stage of deformation at strain rates of $(1-5) \times 10^{-3} \text{ s}^{-1}$ can therefore be explained by the action of diffusion creep. The dynamic grain growth observed at the strain rate of 10^{-2} s^{-1} is considerably more essential and is likely to be caused not only by the action of diffusion and dislocation creep, but also by the migration of grain boundaries that occurs in the longitudinal direction under the action of tensile stresses.

CONCLUSIONS

We investigated the indices of superplasticity and the evolution of the grain structure of the Al–7.6% Mg–0.6% Mn–0.25% Cr alloy in the process of superplastic deformation. The alloy demonstrates relative elongations of $600 \pm 10\%$, $450 \pm 10\%$, and $290 \pm 10\%$ at a temperature of 510°C and deformation rates of 1×10^{-3} , 5×10^{-3} , and $1 \times 10^{-2} \text{ s}^{-1}$, respectively. We observed the dynamic grain growth upon the deformation to 300%, but the grain size is not changed up to failure at the strain rates of 1×10^{-3} and $5 \times 10^{-3} \text{ s}^{-1}$.

After the 100-% deformation, particle-depleted zones were observed in the structure of the samples, which are the result of diffusion creep. With an increase in the deformation rate by an order of magni-

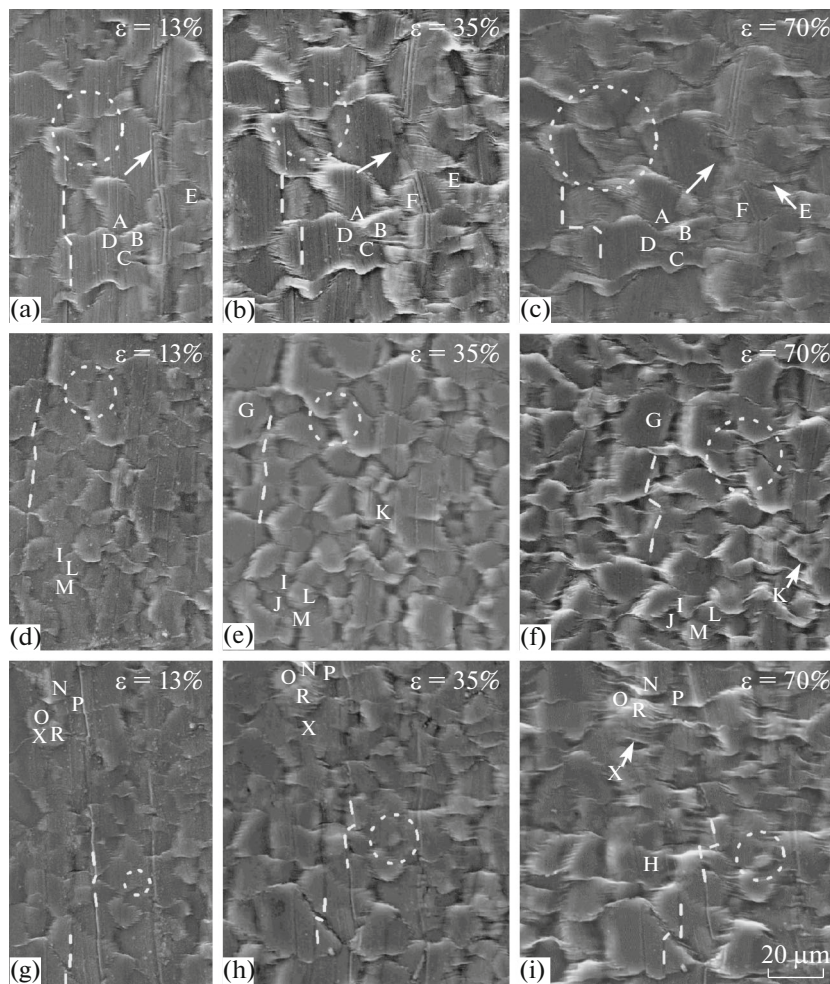


Fig. 6. Evolution of the surface of samples with marker scratches after deformation at the temperature of 510°C and strain rates of (a–c) 1×10^{-3} , (d–f) 5×10^{-3} , and (g–i) $1 \times 10^{-2} \text{ s}^{-1}$. The degree of deformation is indicated in the figure.

tude, from 1×10^{-3} to $1 \times 10^{-2} \text{ s}^{-1}$, the contribution of diffusion creep to the total deformation decreases from 40 to 20%.

Upon the deformation of samples from 13 to 70%, the contribution of grain-boundary sliding estimated based on the evolution of marker scratches on the surface of samples, only weakly depends on the deformation rate and is equal to 20–30%. In the bulk of the samples, after the deformation to 50–100%, we observed signs of dislocation activity, the appearance of dislocation walls; this indicates the important role of dislocation accommodation, which is supposed to be also localized on the periphery of grains in the regions of striated zones.

ACKNOWLEDGMENTS

The work was supported by the Ministry of Education and Science of the Russia Federation in the framework of the Federal task no. 11.7172.2017/8.9 for 2017–2020.

REFERENCES

1. S. Kalpakjian, *Manufacturing engineering and technology*, 3rd ed. (Addison-Wesley Publishing Company, Massachusetts, 1995).
2. T. G. Nieh, J. Wadsworth, and O. D. Sherby, *Superplasticity in Metals and Ceramics* (Cambridge University Press, New York, 2005).
3. K. Sotoudeh and P. S. Bate, “Diffusion creep and superplasticity in aluminium alloys,” *Acta Mater.* **58**, 1909–1920 (2010).
4. I. I. Novikov and V. K. Portnoi, “Superplasticity of alloys with ultrafine grain,” (*Metallurgiya*, Moscow, 1981) [in Russian].
5. H. Masuda, T. Kanazawa, H. Tobe, and E. Sato, “Dynamic anisotropic grain growth during superplasticity in Al–Mg–Mn alloy,” *Scr. Mater.* **149**, 84–87 (2018).
6. R. W. Cahn, P. Haasen, and E. J. Kramer, *Mater. Sci. Technology* (VCH, New York, 1993), Vol. 6.
7. R. M. Cleveland, A. K. Ghosh, and J. R. Bradley, “Comparison of superplastic behavior in two 5083 alu-

- minum alloys,” *Mater. Sci. Eng., A* **351**, 228–236 (2003).
8. K. Zhang and H. Yan, “Deformation behavior of fine-grained 5083 Al alloy at elevated temperature,” *Trans. Nonferrous Met. Soc. China* **19**, 307–311 (2009).
 9. R. Verma, A. K. Ghosh, S. Kim, and C. Kim, “Grain refinement and superplasticity in 5083 Al,” *Mater. Sci., Eng. A* **191**, 143–150 (1995).
 10. S. S. Woo, Y. R. Kim, D. H. Shin, and W. J. Kim, “Effects of Mg concentration on the quasi-superplasticity of coarse-grained Al–Mg alloys,” *Scr. Mater.* **37**, 1351–1358 (1997).
 11. A. A. Kishchik, A. V. Mikhailovskaya, V. S. Levchenko, and V. K. Portnoi, “Formation of microstructure and superplasticity of magnalics,” *Phys. Met. Metallogr.* **118**, 96–103 (2017).
 12. D. Y. Maeng, J. H. Lee, S. I. Hong, and B. S. Chun, “Microstructure and mechanical properties of rapidly solidified Al–7 wt % Mg– X ($X = \text{Cr, Zr or Mn}$) alloys,” *Mater. Sci. Eng., A* **311**, 128–134 (2001).
 13. A. D. Kotov, A. V. Mikhaylovskaya, and V. K. Portnoi, “Effect of the solid-solution composition on the superplasticity characteristics of Al–Zn–Mg–Cu–Ni–Zr alloys,” *Phys. Met. Metallogr.* **115**, 730–735 (2014).
 14. V. K. Portnoi, D. S. Rylov, V. S. Levchenko, and A. V. Mikhaylovskaya, “The influence of chromium on the structure and superplasticity of Al–Mg–Mn alloys,” *J. Alloys Compd.* **581**, 313–317 (2013).
 15. G. T. Langdon, “Grain boundary sliding revisited: Developments in sliding over four decades,” *J. Mater. Sci.* **41**, 597–609 (2006).
 16. E. Alabort, P. Kontis, D. Barba, K. Dragnevski, and R. C. Reed, “On the mechanisms of superplasticity in Ti–6Al–4V,” *Acta Mater.* **105**, 449–463 (2016).
 17. M. A. Rust and R. I. Todd, “Surface studies of Region II superplasticity of AA5083 in shear: Confirmation of diffusion creep, grain neighbor switching and absence of dislocation activity,” *Acta Mater.* **59**, 5159–5170 (2011).
 18. C. M. Cepeda-Jiménez, J. M. García-Infanta, O. A. Ruano, and F. Carreno, “High strain rate superplasticity at intermediate temperatures of the Al7075 alloy severely processed by equal channel angular pressing,” *J. Alloys Compd.* **509**, 9589–9597 (2011).
 19. H. E. Adabbo, G. Gonzalez-Doncel, O. A. Ruano, J. M. Belzunce, and O. D. Sherby, “Strain hardening during superplastic deformation of Al-7475 alloy,” *Mater. Res. Soc.* **3**, 587–594 (1989).
 20. A. V. Mikhaylovskaya, O. A. Yakovtseva, M. N. Sitkina, A. D. Kotov, A. V. Irzhak, S. V. Krymskiy, and V. K. Portnoi, “Comparison between superplastic deformation mechanisms at primary and steady stages of the fine grain AA7475 aluminium alloy,” *Mater. Sci. Eng., A* **718**, 277–286 (2018).
 21. J. R. Spingarn and W. D. Nix, “Diffusion creep and diffusionally accommodated grain rearrangement,” *Acta Metall.* **26**, 1389–1398 (1978).
 22. I. I. Novikov, V. K. Portnoi, and V. S. Levchenko, “Investigation of structural changes during superplastic deformation of Zn–22%Al alloy by replica locating technique,” *Acta Metall.* **29**, 1077–1090 (1981).
 23. O. A. Yakovtseva, A. V. Mikhaylovskaya, A. V. Pozdnyakov, A. D. Kotov, and V. K. Portnoi, “Superplastic deformation behaviour of aluminium containing brasses,” *Mater. Sci. Eng., A* **674**, 135–143 (2016).
 24. W. Wang, M. Yang, D. Yan, P. Jiang, F. Yuan, and X. Wu, “Deformation mechanisms for superplastic behaviors in a dual-phase high specific strength steel with ultrafine grains,” *Mater. Sci. Eng., A* **702**, 133–141 (2017).
 25. O. A. Yakovtseva, A. V. Mikhailovskaya, A. D. Kotov, and V. K. Portnoi, “Effect of alloying on superplasticity of two-phase brasses,” *Phys. Met. Metallogr.* **117**, 742–748 (2016).
 26. C. W. Humpries and N. Ridley, “Cavitation during the superplastic deformation of an α/β brasses,” *J. Mater. Sci.* **13**, 2477–2482 (1978).
 27. O. A. Yakovtseva, A. V. Mikhaylovskaya, A. G. Mochugovskiy, V. V. Cheverikin, and V. K. Portnoi, “Superplastic deformation mechanisms in high magnesium containing aluminum alloy,” *Mater. Sci. Forum* **838–839**, 66–71 (2016).
 28. D. H. Bae and A. K. Ghosh, “Cavity growth during superplastic flow in an Al–Mg alloy: I. Experimental study,” *Acta Mater.* **50**, 993–1009 (2002).
 29. R. Verma, P. A. Friedman, A. K. Ghosh, S. Kim, and C. Kim, “Characterization of superplastic deformation behavior of a fine grain 5083 Al alloy sheet,” *Metall. Mater. Trans. A* **27**, 1889–1898 (1996).
 30. J. J. Blandin, B. Hong, A. Varloteaux, M. Suery, and G. L’esperance, “Effect of the nature of grain boundary regions on cavitation of a superplastically deformed aluminium,” *Acta Mater.* **44**, 2317–2326 (1996).
 31. *Determination of Superplasticity Indicators: Methodical Recommendation MR 252-31-86* (VILS, Moscow, 1986) [in Russian].
 32. V. K. Portnoi and I. I. Novikov, “Evaluation of grain boundary sliding contribution to the total strain during superplastic deformation,” *Scr. Mater.* **40**, 39–43 (1999).

Translated by S. Gorin